



Chitosan nonwoven fabric composited calcium alginate and adenosine diphosphate as a hemostatic bandage for acute bleeding wounds

Jianmin Yang ^{a,b,*}, Fengying Cai ^a, Yicheng Lv ^a, Ting Jiang ^a, Xingkai Zhao ^a, Xueli Hu ^a, Yunquan Zheng ^b, Xianai Shi ^{a,b,*}

^a College of Biological Science and Engineering, Fuzhou University, No. 2 Xueyuan Road, Fuzhou 350108, China

^b Fujian Key Laboratory of Medical Instrument and Pharmaceutical Technology, Fuzhou University, No. 2 Xueyuan Road, Fuzhou 350108, China



ARTICLE INFO

Keywords:

Chitosan nonwoven fabric
Hemostatic bandage
Synergistic hemostatic
Acute bleeding wound
Hemostatic mechanisms

ABSTRACT

Acute bleeding following accidental injury is a leading cause of mortality. However, conventional hemostatic bandages impede wound healing by inducing excessive blood loss, dehydration, and adherence to granulation tissue. Strategies such as incorporating active hemostatic agents and implementing chemical modifications can augment the properties of these bandages. Nevertheless, the presence of remote thrombosis and initiators may pose risks to human health. Here, a hemostatic bandage was developed by physically combined chitosan nonwoven fabric, calcium alginate sponge, and adenosine diphosphate. The presented hemostatic bandage not only exhibits active and passive mechanisms for promoting clotting but also demonstrates excellent mechanical properties, breathability, ease of removal without causing damage to the wound bed or surrounding tissues, as well as maintaining an optimal moist environment conducive to wound healing. *In vitro* evaluation results indicated that the hemostatic bandage possesses favorable cytocompatibility with low levels of hemolysis. Furthermore, it effectively aggregates various blood cells while activating platelets synergistically to promote both extrinsic and intrinsic coagulation pathways. In an *in vivo* rat model study involving liver laceration and femoral artery injury scenarios, our developed hemostatic bandage demonstrated rapid clot formation capabilities along with reduced blood loss compared to commercially available fabrics.

1. Introduction

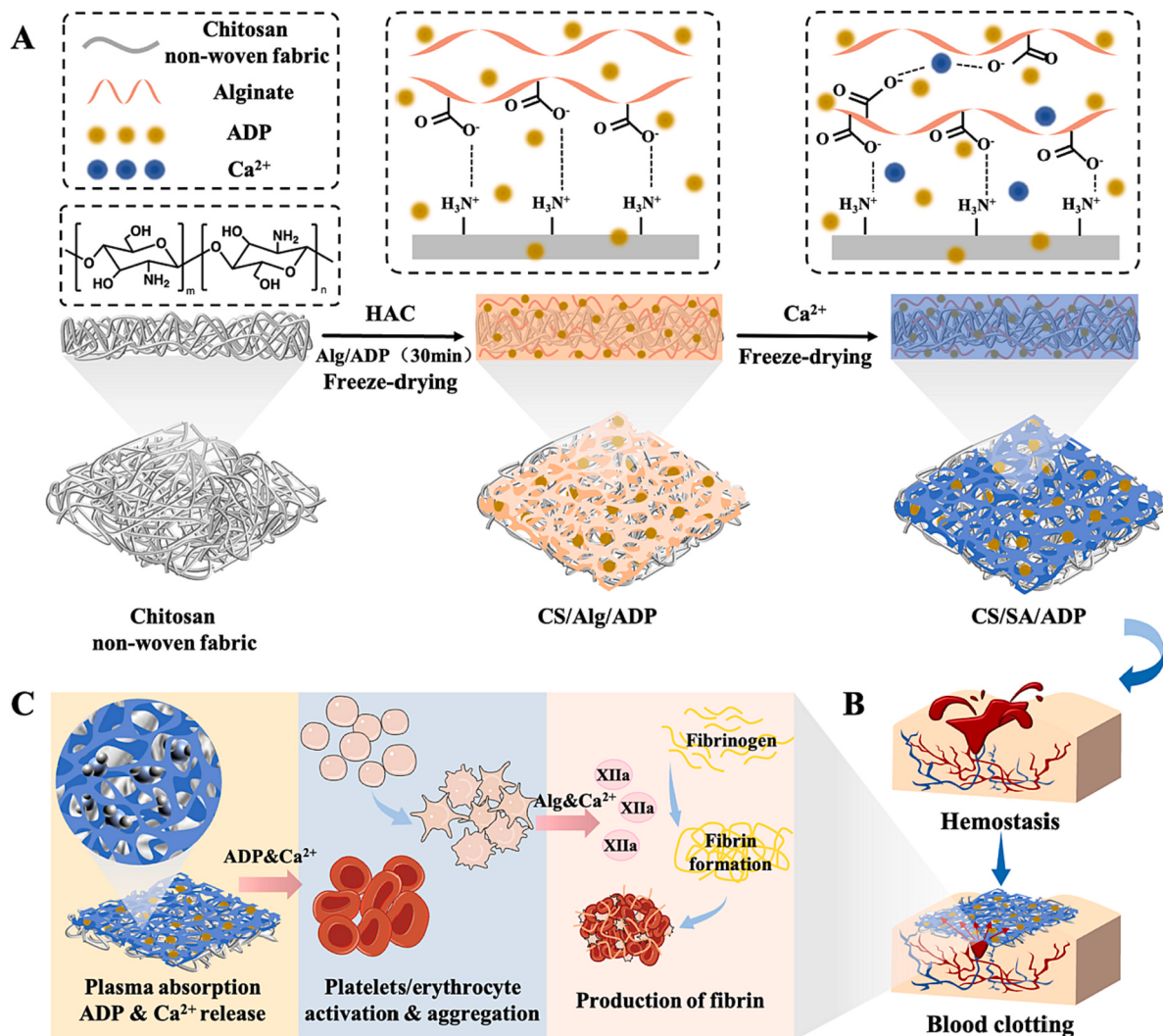
Acute massive blood loss will lead to hypothermia, internal organ failure, metabolic acidosis, and other symptoms; which is a cause of death in wars, surgery, traffic accidents, and natural disasters [1,2]. Thus, using an effective hemostatic material in the early stages of bleeding is crucial for saving patients' lives and extending resuscitation time [3,4]. Although various types of hemostatic materials including sponges, powders, and hydrogels have been developed, hemostatic bandages remain the most widely employed strategy for controlling traumatic bleeding [5–7]. Hemostatic bandages have been used as effective exterior hemostatic dressings due to their breathability, safety, nonallergenicity, absorption, and ease of application [8]. However, traditional hemostatic bandages primarily depend on the hydrophilicity, porous structure, and capillary action among fibers to concentrate blood cells, thereby requiring relatively long hemostasis time and easily causing excessive blood loss [9,10]. Furthermore, these bandages fail to

maintain wound moisture levels effectively while often adhering to the wound surface which can lead to dehydration and delayed wound healing [11–13]. Therefore, the development of anti-adhesive hemostatic bandages that also maintain wound moisture levels remains a significant challenge.

Recently, several studies have been conducted to improve the hemostatic properties of bandages through reduction in blood loss and hemostasis time. Consequently, various advanced hemostatic bandages have been developed [14–16]. Notably, chitosan-based hemostatic dressings such as HemCon® bandages, Celox® Rapid, and ChitoGauze®, have gained widespread utilization in military, emergency care, hospital, and other related fields [17,18]. Due to the positively charged amino groups on its skeleton, chitosan can interact electrostatically with the negatively charged erythrocyte cell membranes, thus promoting the aggregation of erythrocytes. In addition, chitosan has good biocompatibility, biodegradability, antibacterial, anti-inflammatory, and anti-tumor activities, thus it has an important application value in the field of

* Corresponding authors at: College of Biological Science and Engineering, Fuzhou University, No. 2 Xueyuan Road, Fuzhou 350108, China.

E-mail addresses: jmyang@fzu.edu.cn (J. Yang), shixa@fzu.edu.cn (X. Shi).



Scheme 1. Fabrication and application schematic of the hemostatic bandage CS/SA/ADP. (A) Fabrication process of the hemostatic bandage. (B) Application of the hemostatic bandage for acute bleeding wounds. (C) Mechanism underlying coagulation facilitated by the hemostatic bandage.

tissue engineering and regenerative medicine [19–21]. However, the erythrocyte aggregates formed by chitosan fabric during hemostasis are inherently unstable and may cause secondary bleeding upon bandage dislodgement.

To address these issues, various strategies involving chemical modifications and the incorporation of active coagulants into fabrics have been explored to enhance the hemostatic efficacy of bandages [22–24]. However, these approaches still fall short in meeting the requirements of cost-effectiveness, safety, and structural stability. For instance, the application of coagulants such as thrombin, fibrinogen, kaolin, and zeolite are hindered due to their high cost, immunogenicity, potential risk of viral transmission, and safety issues associated with distal thrombosis [25–27]. Alternatively, adenosine diphosphate (ADP) has gained significant attention as a physiologically relevant platelet agonist. ADP is the first discovered important agonist for platelet aggregation that is mainly stored in dense granules of platelets [28,29]. It can stimulate the secretion of dense particles, induce platelet aggregation and shape change, and contribute to the formation and stability of thrombosis during hemostasis process [30]. Although ADP has significant procoagulant potential, there have been limited reports on its application in hemostasis [31,32].

Fabrics are extensively utilized in the fabrication of hemostatic bandages owing to their good mechanical properties, high porosity, and extracellular matrix-like structure. Regrettably, their inadequate

absorption and water retention characteristics can potentially result in wound dehydration and adhesion of the material to the injured surface during application [33–35]. Hence, the incorporation of sponges, membranes, or creams into fabric matrices can enhance hemostatic properties and cater to diverse requirements during wound healing [36–38]. Compared to other materials, sponge offers numerous advantages such as porosity, hydrophilicity, and moisture retention [39–41]. For instance, calcium alginate sponges undergo transformation from insoluble calcium alginate to sodium alginate hydrogel during hemostasis, facilitating easy removal from the wound site and reducing pain. Additionally, negatively charged alginates can expedite coagulation by activating coagulation factor XII. Furthermore, the addition of the cross-linking agent CaCl_2 enhances coagulation efficiency through extrinsic and intrinsic hemostasis [42]. However, the limited mechanical strength of alginate sponges restricts their application scope [43]. Therefore, we propose a novel approach that combines fabrics with calcium alginate sponges to overcome these limitations and develop an advanced hemostatic material. The synergistic advantages of fabric and sponge in terms of their structure and composition are harnessed to achieve optimal hemostasis performance and create an ideal moist environment for wound healing.

In this study, we developed a hemostatic bandage (CS/SA/ADP) with synergistic advantages for the management of acute bleeding wounds (**Scheme 1**). In preparing the hemostatic bandages, chitosan nonwoven

fabric was initially immersed in a mixed solution of sodium alginate and ADP, followed by cross-linking using Ca^{2+} to obtain the desired product. Given its unique fabric mesh structure and spongy properties, the hemostatic bandage not only efficiently absorbs wound exudate and provides a moist microenvironment, but also exhibits good mechanical strength and breathability. Moreover, the chitosan nonwoven fabric in the hemostatic bandage facilitates primary hemostasis, blood absorption, and concentration of clotting components. Additionally, sodium alginate, ADP, and Ca^{2+} play crucial roles in promoting platelet adsorption and accelerate coagulation. Here, the air permeability, absorbency, and mechanical properties of hemostatic bandages were characterized. *In vitro* coagulation properties of the hemostatic bandage were investigated by examining the erythrocyte/platelet aggregation activation, coagulation pathways, and whole blood coagulation capacity. The peeling behavior of the hemostatic bandage was evaluated in rat back wounds, while its hemostatic effect was verified through measurements of hemostasis time and blood loss in a rat liver laceration and femoral artery injury model. Furthermore, the biocompatibility of the hemostatic bandage was assessed through subcutaneous implantation and blood routine analysis.

2. Materials and methods

2.1. Materials

Chitosan nonwoven fabric (120 g/m^2 , degree of deacetylation = 95.3 %, Mw ~ 1000 kDa) was purchased from Hismer Biotechnology Co., Ltd. (Shandong, China). Glacial acetic acid and calcium chloride (CaCl_2) were obtained from Sinopharm Chemical Reagent Co., Ltd. (Shanghai, China). Sodium alginate (viscosity = $200 \pm 20 \text{ cps}$, Mw = 32–250 kDa) was purchased from Macklin Biochemical Co., Ltd. (Shanghai, China). ADP was obtained from Aladdin Biochemical Technology Co., Ltd. (Shanghai, China). Mouse embryonic fibroblasts (NIH-3 T3) were purchased from Dingguo Biotechnology Co., Ltd. (Beijing, China). Human umbilical vein endothelial cells (HUVECs) were obtained from Enzyme Research Biotechnology Co., Ltd. (Shanghai, China). Live/dead assay kit and cell counting kit-8 were purchased from Beyotime Biotechnology Co., Ltd. (Shanghai, China). Lactate dehydrogenase (LDH) activity assay kit, prothrombin time (PT) assay kit, and activated partial thromboplastin time (APTT) assay kit were purchased from Solarbio Science & Technology Co., Ltd. Glutaric dialdehyde (GA), ethanol, and paraformaldehyde were obtained from Sinopharm Chemical Reagent Co., Ltd. (Shanghai, China). Male Sprague Dawley (SD) rats with weight of 230–250 g was obtained from Slack Experimental Animal Co., Ltd. (Shanghai, China). ChitoGauze XR® Pro and ChitoSAM™ 100 were purchased from Sibaike Biotechnology Co., Ltd. (Nanjing, China). Sorbalgon® was obtained from Bohmann Trading Co., Ltd. (Shanghai, China). The reagents used in the experiments were of analytical grade, and they need not to be purified once again.

2.2. Characterizations

The morphology of the hemostatic bandage was observed using a scanning electron microscope (Nova NanoSEM 230, Japan) at 20 kv. Elemental mapping of the hemostatic bandages was characterized by energy dispersive spectrometer (XFlash Detector 6|30, Germany). The chemical structure of the hemostatic bandages was characterized by Fourier transform infrared spectrometer (FT-IR, Nicolet iS50, USA). Thermal stability of hemostatic bandages was analyzed using thermogravimetric analysis on a simultaneous thermal analyzer (STA449C, Germany). Tensile strength and elongation characteristics were measured using a universal material testing machine (TA. XT PLUS, SMS, U.K.), with a $1 \times 3 \text{ cm}$ hemostatic bandages tested at a speed of 10 mm/min. The blood/water contact angle of the samples was assessed using an Easy Drop water contact angle meter (HVS430W, China) by adding drops of blood/water (5 μL) to the sample surface and measuring

both the contact angle and penetration effect.

2.3. Preparation of composite hemostatic materials

The chitosan nonwoven fabric was initially treated with a 1 % acetic acid solution ($\text{pH} = 5.5$) and subsequently immersed in a 0.75 % sodium alginate solution. After a duration of 20 min, the samples were removed from the sodium alginate solution and rinsed with distilled water. Freeze drying was then conducted, followed by soaking the sample in a 0.2 M CaCl_2 . After another round of freeze drying, the CS/SA composite hemostatic dressing was obtained. Additionally, the sodium alginate sponge underwent soaking in CaCl_2 followed by subsequent freeze drying to yield an SA hemostatic sponge. To prepare SA/ADP and CS/SA/ADP hemostatic bandages, incorporation of 200 mM ADP into the sodium alginate solution was carried out using the aforementioned method.

2.4. Hemolytic activity test

Freshly collected SD rat blood containing anticoagulant was centrifuged at 1500 rpm for 10 min. The supernatant was discarded, and the red blood cells were washed with saline and subsequently diluted into a 5 % erythrocyte suspension. Subsequently, pre-warmed sample (10 mg) was added to 5 % erythrocyte suspension (1 mL). After incubation at 37 °C for 1 h, the samples were centrifuged at 1000 rpm for 10 min to precipitate the erythrocytes. The supernatant, containing the released hemoglobin (HA) from lysed erythrocytes, was collected. The absorbance of the supernatant at a wavelength of 540 nm was measured, with saline solution as a blank control and 0.1 % Triton X-100 as a positive control. The hemolysis rate was calculated using the following equation: Hemolysis rate (%) = $(\text{OD}_{\text{sample}} - \text{OD}_{\text{control}})/(\text{OD}_{\text{positive}} - \text{OD}_{\text{control}}) \times 100 \%$.

2.5. In vitro whole blood coagulation test

The *in vitro* coagulation rate of different samples was compared by performing all tests in tubes at 37 °C. The pre-warmed sample (10 mg) was added to 100 μL of recalcified blood (0.2 M CaCl_2 : blood = 1: 10) and incubated for specific time intervals (30, 60, 90, 120, and 180 s). Afterward, 1 mL of deionized water was gently added to terminate the reaction without disturbing the clot. The released HA from free erythrocytes was measured as the method mentioned before. The unclotted state was observed at time point zero seconds (HA_0), subsequently, the amount of hemoglobin in the unclotted erythrocytes was measured at t seconds (HA_t). The relative hemoglobin (RHA) value can be calculated using the following formula: $\text{RHA} (\%) = \text{HA}_t / \text{HA}_0 \times 100 \%$.

Similarly, the pre-warmed sample (10 mg) was supplemented with 200 μL of recalcified blood and subjected to shaken. Subsequently, the centrifuge tube was periodically tilted every 10 s to monitor coagulation. The duration from the moment when samples came into contact with blood until complete cessation of flow was recorded, while employing 200 μL of recalcified blood as a blank control.

2.6. In vitro vascular injury simulation hemostasis test

A polyethylene hose with an inner diameter of 7.8 mm was incised to measure 5 mm × 8 mm, and a hemostatic bandage was applied to cover the wound. Wound covered with a chitosan nonwoven fabric served as a control. The vascular model was weighed prior to the experiment. Coagulation was initiated by mixing citrated blood with CaCl_2 (0.2 M), and 2 mL of blood was added to the polyethylene hose placed in a Petri dish. After 10 min, the polyethylene hose was removed from the Petri dish and the increase in weight of the dish due to blood leakage as well as the increase in weight of the material was measured as blood loss.

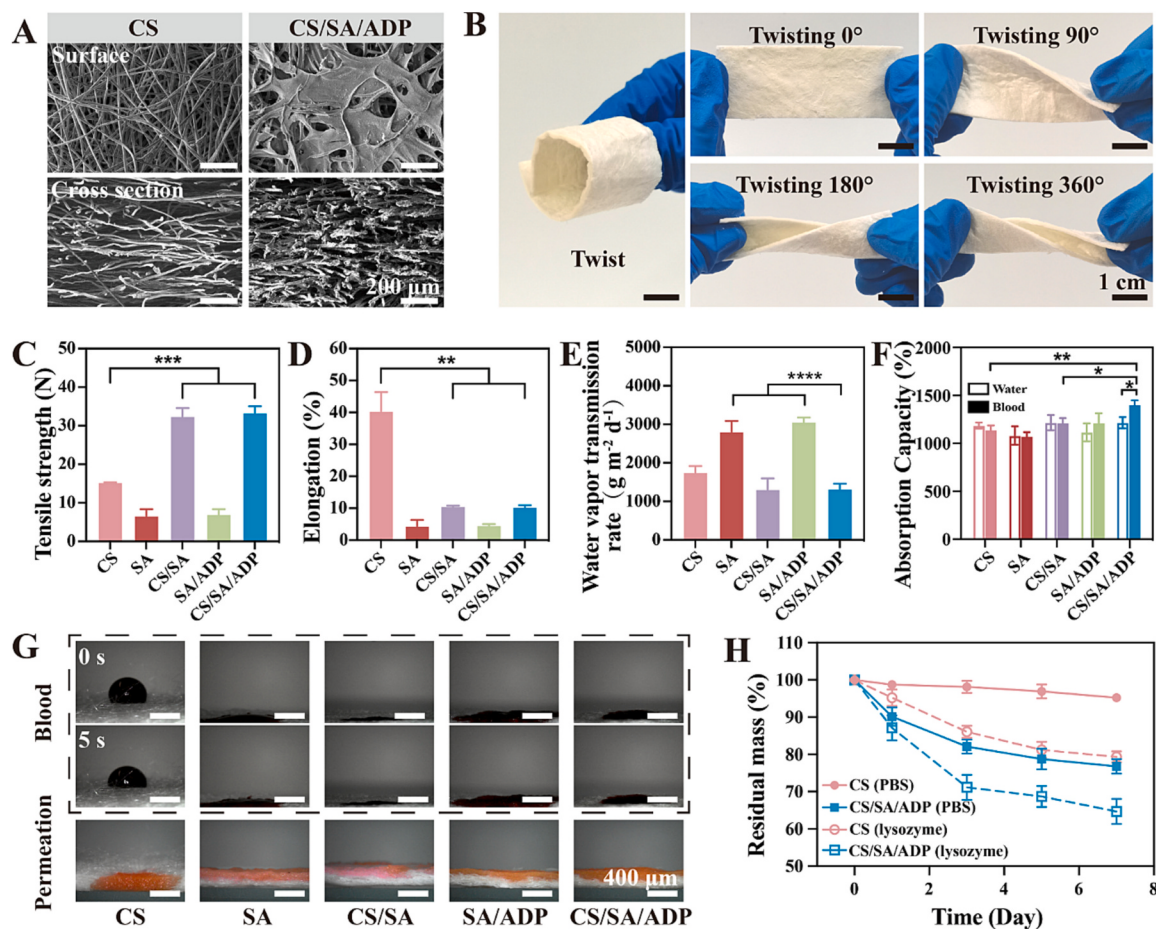


Fig. 1. Characterization of the hemostatic bandage. (A) Surface and cross-sectional SEM images of CS nonwoven fabric and CS/SA/ADP. (B) Photographs of CS/SA/ADP with different extents of *in situ* twist. (C) Tensile strength and (D) elongation at break of various hemostatic bandages. (E) Water vapor transmission rate of hemostatic bandages. (F) Water/blood absorption capacity. (G) Blood contact angle and penetration effect of different types of hemostatic bandages. (H) *In vitro* biodegradation of CS and CS/SA/ADP by PBS and lysozyme.

2.7. Erythrocyte and platelet adhesion

Freshly collected SD rat blood containing anticoagulant was centrifuged at 1500 rpm for 10 min to isolated red blood cell (RBC) and platelet-rich plasma (PRP). RBC were diluted with PBS at a volume ratio of 1:1, and 150 μ L of RBC was incubated with each sample for 30 min at 37 °C, and 150 μ L RBC was used as control. Afterward, the unadhered erythrocytes were removed by rinsing with PBS, followed by lysis of the adhered erythrocytes on the material with 1 mL of deionized water. The absorbance of the lysate at a wavelength of 540 nm was measured. The erythrocyte adhesion rate is calculated as follows: RBC adhesion rate (%) = $OD_{Sample}/OD_{Control} \times 100\%$.

Additionally, erythrocytes were fixed with 2.5 % (v/v) GA/PBS for 3 h, followed by two rinses with deionized water and dehydration using sequential ethanol solutions (60 %, 70 %, 80 %, 90 %, and 100 %) for 15 min each. After drying, the adhesion of RBC on the hemostatic bandages was observed by SEM.

For platelet adhesion analysis, 200 μ L of PRP was co-incubated with each sample at 37 °C for 30 min and subsequently washed with PBS to remove unadhered platelets. Afterward, 1 mL of 1 % Triton X-100 was added and lysed at 37 °C for 1 h. Finally, the activity of platelet LDH was evaluated using an LDH assay kit at a wavelength 450 nm. Platelet adhesion was calculated by plotting a standard curve. PRP without any material was used as a control. The platelet adhesion rate is calculated as follows: Platelet adhesion rate (%) = $OD_{Sample}/OD_{Control} \times 100\%$. Furthermore, platelet aggregation on the hemostatic bandages was also observed by SEM.

2.8. APTT and PT assays

The coagulation activation pathway of the hemostatic bandages was assessed using APTT and PT assay kits. Whole blood from healthy SD rats was centrifuged at 3000 rpm for 10 min, and the supernatant was removed to obtain platelet-poor plasma (PPP). For the APTT assay, 10 mg of the sample was incubated with 100 μ L of PPP at 37 °C for 3 min, followed by the addition of 100 μ L of APTT reagent. After incubation 5 min at 37 °C with gentle mixing, 100 μ L of warmed 25 mM CaCl₂ solution was added, and the blood clotting time was recorded. For the PT assay, the samples were incubated with 100 μ L of PPP at 37 °C for 3 min, followed by the addition of 100 μ L of PT reagent, and the time required for PPP clotting was recorded.

2.9. Peel force measurement

All animal experiments followed strictly the requirements of the National Research Council's Guide for the Care and Use of Laboratory Animals (8th edition) and were formally approved by the Animal Ethics Committee of Fuzhou University. During the experimental period, all animals had free access to food and water.

The hair on the back of the anesthetized SD rats was removed, and the area was disinfected with iodophor. A surgical blade was used to cut 1 cm on each side of the midline of the rat's back, followed by application of a hemostatic bandage measuring 35 mm × 15 mm to cover the wound site. After allowing approximately 1 h for clot formation and maturation, the peak force required for peeling off the bandage was

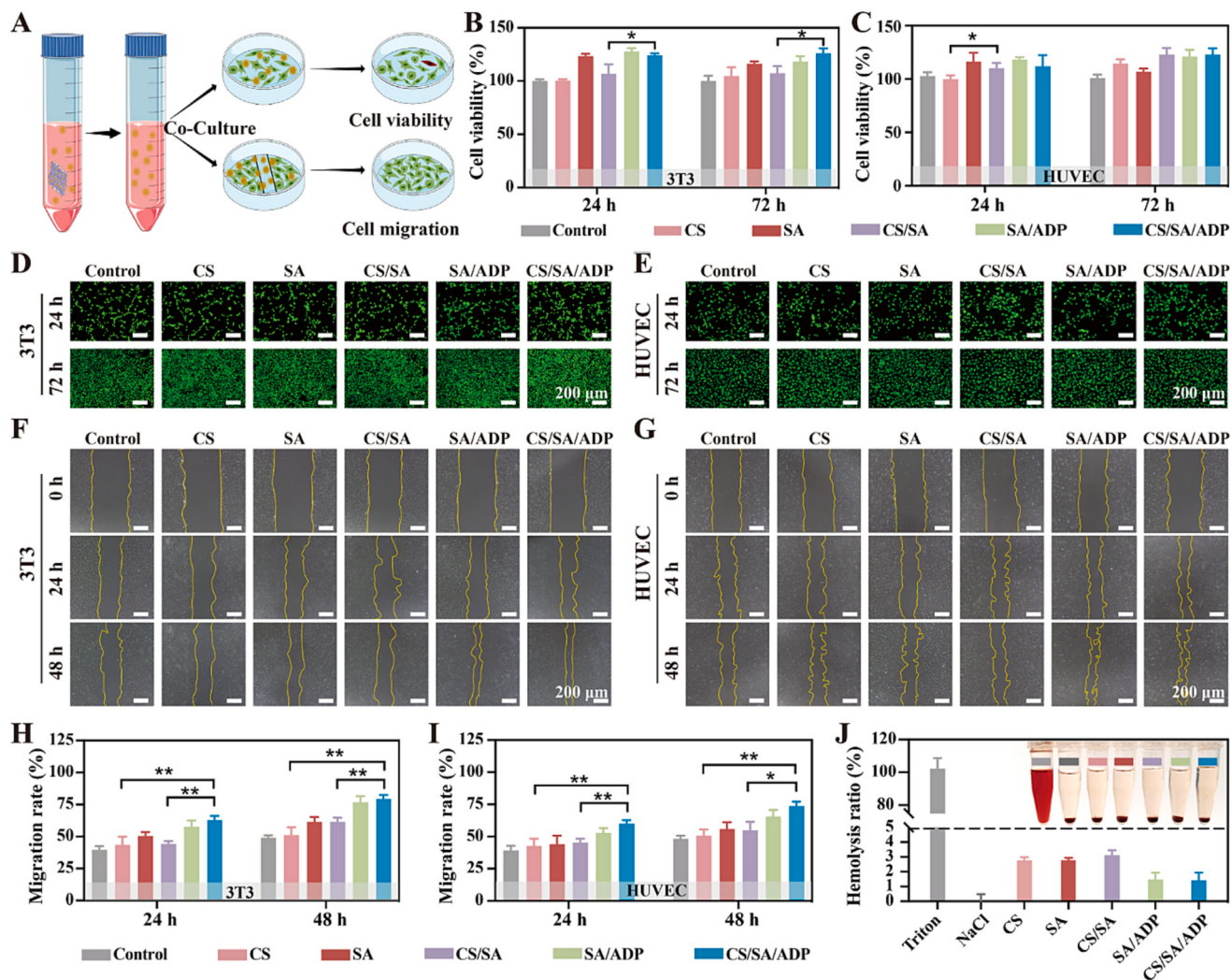


Fig. 2. Cytocompatibility and hemolytic assays of hemostatic bandages. (A) Schematic diagram of the co-culture of material extract and cells. The cell survival rate of (B) 3T3 and (C) HUVEC cells. Live/dead staining analysis of (D) 3T3 and (E) HUVEC cells. (F&G) Migration images and (H&I) migration rates of 3T3 and HUVEC cells. (J) Hemolysis rate of different hemostatic bandages.

measured using a digital push-pull meter.

2.10. In vivo hemostatic capability

SD rats were utilized to establish models of liver laceration and leg femoral artery hemorrhage. Rats were initially anesthetized via intraperitoneal injection of sodium pentobarbital (1 %, 40 mg/kg) and immobilized. For the rat liver laceration hemorrhage model, abdominal hair was removed prior to incising the abdominal epithelial tissue to expose the liver. A wound measuring 1 cm in length and 0.5 cm in depth was then created on the left lobe of the liver. Subsequently, a pre-weighed sample measuring 3 cm × 3 cm was applied over the wound site. The hemostasis time was recorded, and blood loss was calculated by weighing the sample after achieving hemostasis. Following hemostasis, the bandage was removed and the liver repositioned. After a period of 7 days, H&E and Masson staining were performed on excised liver samples from the incision site to evaluate any potential impact of bandage residue on hepatic tissues.

The leg was prepared for the rat femoral artery model, and the femoral artery was exposed and punctured using a 20 G needle. The pre-weighed sample was covered, and gentle pressure was applied to the bleeding site. Hemostasis time and blood loss were recorded.

2.11. Histocompatibility evaluation

SD rats were anesthetized with sodium pentobarbital. After shaving the hair on the back, a 1 × 1 cm hemostatic bandage was implanted under the skin on the back of the rats, sutured immediately, and sterilized with iodophor. Blood samples were collected from rats on day 7 and day 21 for routine blood tests, and skin reactions of each group were observed. Subsequently, the rats were euthanized, and tissue samples were excised and fixed with 4 % paraformaldehyde for preservation. The histocompatibility of the materials was assessed through H&E staining and immunofluorescence imaging.

2.12. Statistical analysis

The results presented in this study were obtained through at least three independent experiments and are reported as mean values ± standard derivation. One-way analysis of variance (ANOVA) and student *t*-test was used for the treatment comparison. Comparisons with **p* < 0.05, ***p* < 0.01, ****p* < 0.001 and *****p* < 0.0001 were considered statistically significant, the NS represented no significant difference.

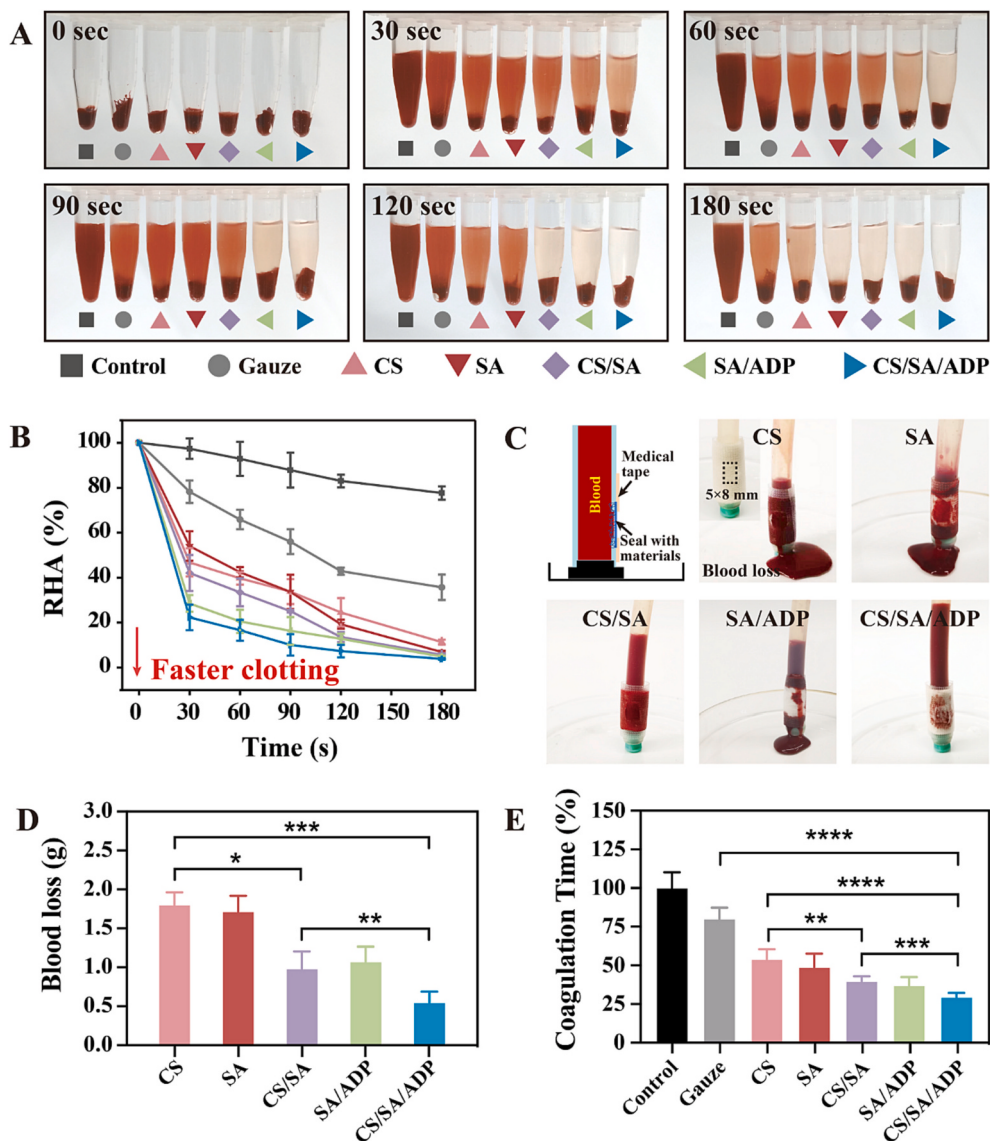


Fig. 3. *In vitro* hemostatic performance. (A) Photographs of *in vitro* blood coagulation assay and (B) corresponding statistical plots of RHAs for control, gauze, CS, SA, CS/SA, SA/ADP, and CS/SA/ADP at time intervals of 0, 30, 60, 90, 120, and 180 s. (C) Photographs of blood loss at 10 min in an *in vitro* simulated vascular injury model and (D) quantitative analysis. (E) Coagulation time.

3. Results and discussion

3.1. Preparation and characterization of hemostatic bandages

Chitosan nonwoven fabric is composed of randomly oriented fibers (Fig. 1A). A sponge layer can be observed on the surface, which is embedded in the nonwoven fabric in CS/SA/ADP. The EDS mapping and FT-IR results confirmed the successful binding of sodium alginate, ADP, and Ca^{2+} to the chitosan nonwoven fabric (Figs. S1 and S2). As shown in Fig. 1B, the hemostatic bandage has good flexibility (capable of twisting 360° *in situ*), which is beneficial for hemostasis at different wound sites. Moreover, CS/SA/ADP has higher tensile strength and lower elongation compared to CS alone (Fig. 1C and D). The incorporation of sodium alginate and Ca^{2+} into the hemostatic bandage enhances its structural compactness and mechanical properties, resulting in reduced elongation. Consequently, the prepared hemostatic bandages maintain their shape at wound sites extended periods, thereby facilitating rapid wound healing following hemostasis [44].

Hemostatic bandages should possess absorbent and breathable properties to prevent dehydration and excessive accumulation of

exudate at the wound site [45,46]. As shown in Fig. 1E, SA and SA/ADP sponge exhibit a higher water vapor transmission rate, while CS/SA/ADP demonstrate reduced permeability. The reason can be attributed to the increased density of the CS/SA/ADP due to infiltration of calcium alginate into the chitosan nonwoven fabric pores, thereby impeding air flow and subsequently reducing the rate of water vapor transmission. However, CS/SA/ADP maintains good air permeability, facilitating oxygen exchange between the wound and external environment. Blood/water adsorption test showed that CS/SA/ADP adsorbed more red blood cells and platelets than water, and was also significantly higher than CS/SA blood adsorption (Fig. 1F). This suggests that ADP can effectively adsorb blood cells and promote their aggregation on the hemostatic bandage surface. Furthermore, the contact angle measurement as well as diffusion analysis demonstrated rapid absorption and diffusion of blood when added to CS/SA/ADP (Fig. 1G). However, CS maintains a certain contact angle within 5 s due to its inherent hydrophobicity. Therefore, the addition of calcium alginate improves the hydrophilicity of the hemostatic bandage.

Additionally, the degradation test results demonstrated that CS exhibited limited degradability in PBS, whereas the CS/SA/ADP

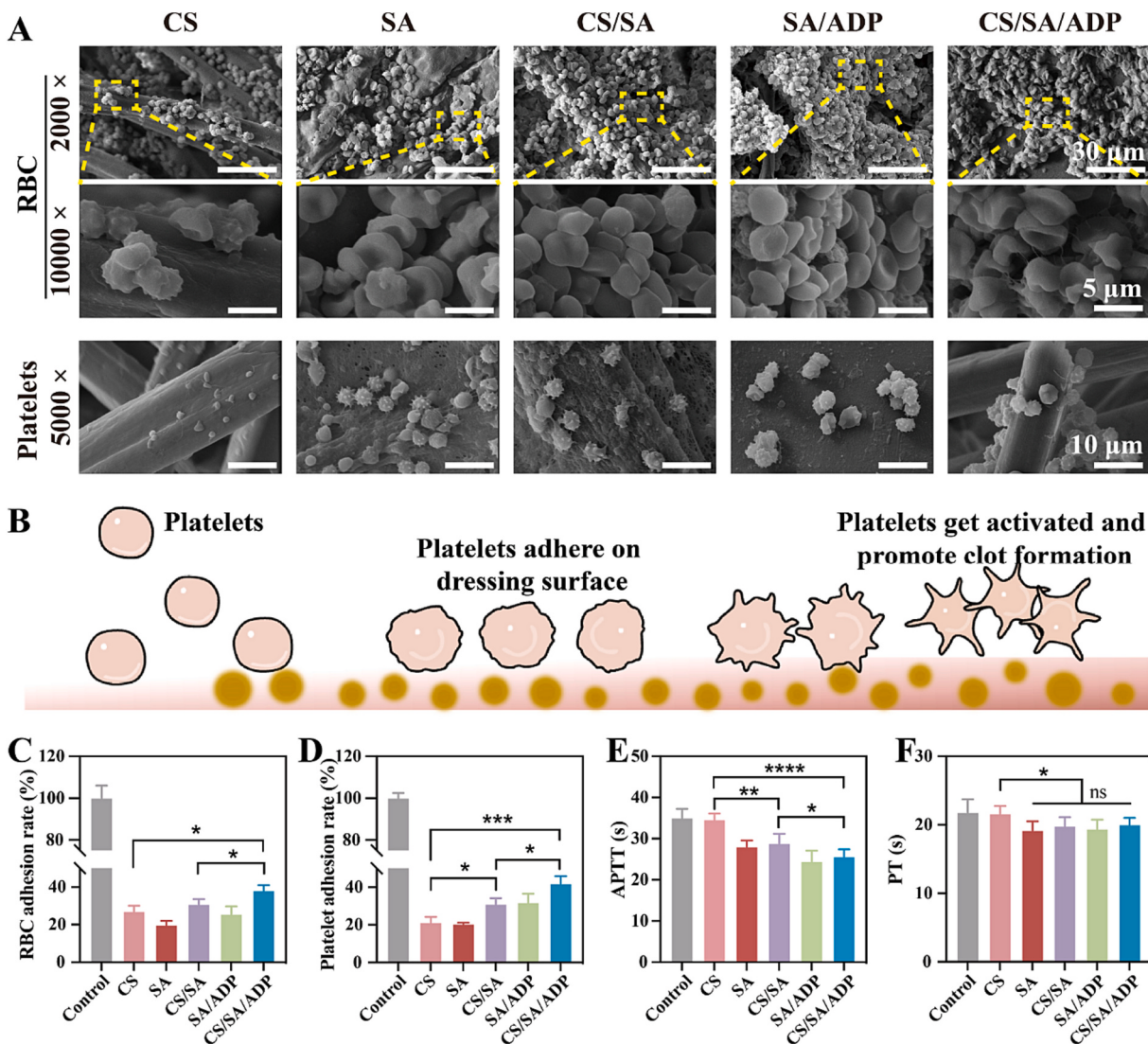


Fig. 4. *In vitro* hemostatic mechanism. (A) SEM images of erythrocyte and platelet adhesion to different material surfaces. (B) Schematic representation of the coagulation mechanism of the interaction between ADP and platelets, with platelets adhering to the surface of the hemostatic bandages and subsequently being activated. *In vitro* mechanistic studies of hemostatic bandages for (C) RBC and (b) platelet adhesion. (E) APTT and (F) PT studies.

experienced a weight loss of about 23 % by day 7 (Fig. 1H). The reduction in weight of CS/SA/ADP was primarily attributed to calcium alginate dissociation. Both CS and CS/SA/ADP degraded significantly in the presence of lysozyme solution, with the latter retaining approximately 65 % of its initial weight by day 7. Furthermore, thermogravimetric analysis revealed that the CS/SA/ADP possessed good thermal stability (Fig. S3).

3.2. Cytocompatibility and hemolytic properties

The cytocompatibility of hemostatic bandage was investigated by cell viability and cell migration using 3T3 and HUVEC as cell models (Fig. 2A). The extracts from the hemostatic bandage did not exhibit any cytotoxic effects on both 3T3 and HUVEC cells, with cell viability ranging from 95 % to 130 % for both models (Fig. 2B and C). Moreover, the live/dead fluorescence images showed that cells cultured in different extract groups displayed normal growth patterns, exhibiting comparable morphology and viability to those in the control group (Fig. 2D and E). These findings indicated that the good cytocompatibility of the prepared hemostatic bandages.

As depicted in Fig. 2F and G, the CS/SA/ADP treatment significantly

enhanced the cell migration compared to the control group. In particular, CS/SA/ADP showed a relative scratch closure of 74 % - 80 % for both types of cells at 48 h, whereas the CS group demonstrated only about 50 % (Fig. 2H and I). Notably, it was observed that CS/SA/ADP promoted wound healing more effectively than CS/SA alone due to ADP's ability to activate signaling pathways upon binding to cell surface receptors involved in biobehavioral processes such as cell activation, migration, and proliferation [47,48]. These results indicated that the prepared hemostatic bandage could promote wound healing. Furthermore, no rupture or lysis of red blood cells occurred after the contact between the prepared samples and blood (Fig. 2J). Moreover, the measured hemolysis rate was <5 %, indicating high hemocompatibility of hemostatic bandages.

3.3. *In vitro* hemostatic properties

The levels of free HA in red blood cells serve as indicators of coagulation, and the absorbance value are normalized to RHA [49]. As shown in Fig. 3A, the RHA level decreased at a faster rate in the CS/SA/ADP group compared to other groups, suggesting an accelerated coagulation process. Approximately 77.67 % ± 5.72 % of erythrocytes were

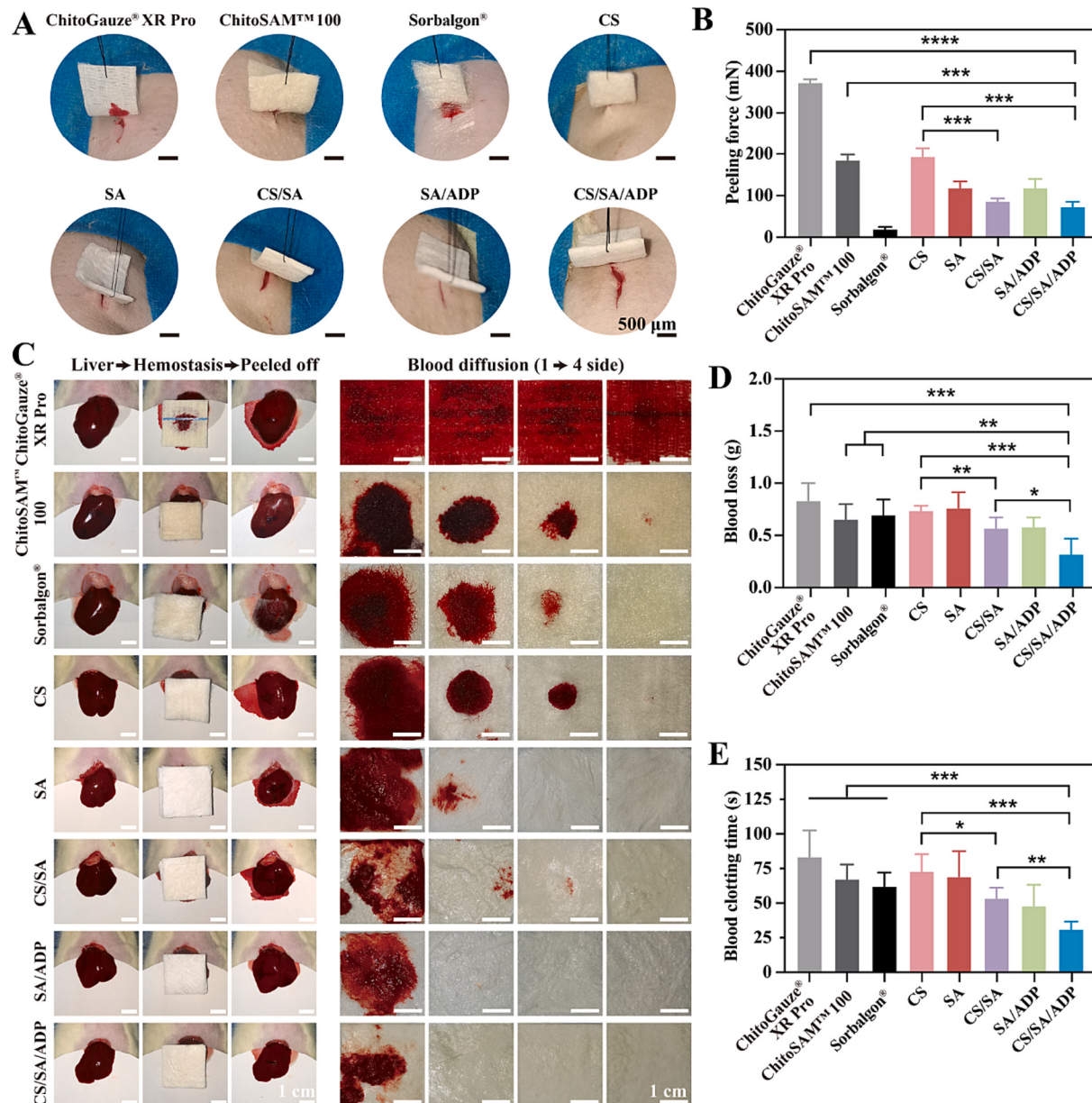


Fig. 5. Evaluation of peeling force and *in vivo* hemostatic properties. (A) Photographs for peeling hemostatic materials from the wound site. (B) Peak peeling force of different hemostatic materials. (C) Photographs of hemostasis of rat liver with different hemostatic dressings and the diffusion/permeation of blood in the hemostatic dressing, where the first side corresponds to immediate wound contact and fourth side represents outermost layer exposure. Quantification of (D) blood loss and (E) hemostasis time in the rat liver hemorrhage model.

entrapped within the clot in the CS/SA/ADP group at 30 s, whereas this percentage was $57.92\% \pm 7.99\%$ in the CS/SA group (Fig. 3B). Furthermore, analysis of RHA values in both SA and SA/ADP groups confirmed that ADP can enhance blood coagulation under *in vitro* conditions.

In order to validate the blood loss of CS/SA/ADP at the injury site *in vitro*, a polyethylene hose was filled with blood and punctured on the side to simulate a bleeding wound. As shown in Fig. 3C and D, CS exhibited significant blood penetration resulting in a blood loss of 1.80 ± 0.16 g, while CS/SA measured as 0.98 ± 0.22 g. Remarkably, CS/SA/ADP displayed minimal blood loss (0.55 ± 0.14 g), representing an approximate three-fold reduction compared to the CS group. In addition, the *in vitro* evaluation of whole blood clotting time was conducted. The untreated whole blood exhibited a clotting time conversion rate of 100 % (Fig. 3E). CS, CS/SA, and CS/SA/ADP demonstrated reduced clotting times of $53.98\% \pm 6.40\%$, $39.69\% \pm 3.24\%$, and $29.44\% \pm 2.69\%$,

respectively. This reduction in clotting time can be attributed to the primary hemostatic function of CS through blood cell absorption, independent of the coagulation system [50]. However, when CS/SA/ADP absorbs blood, it releases ADP and Ca^{2+} , triggering a cascade reaction within the coagulation pathway. The combination of active hemostasis and passive hemostasis significantly enhances hemostasis efficiency. It is noteworthy that alginate also contributes to an enhanced procoagulant effect [51].

Blood cell aggregation has been reported to be an important factor in primary hemostasis. To confirm the hemostatic mechanism of the hemostatic bandage, the interaction between erythrocytes/platelets and the hemostatic material was observed using SEM. As shown in Fig. 4A, a substantial number of blood cells adhered to hemostatic materials while maintaining their biconcave disk shape. Similarly, platelet adhesion to these hemostatic materials was also observed. Furthermore, there was a significant increase in platelet aggregation and pseudopodia formation

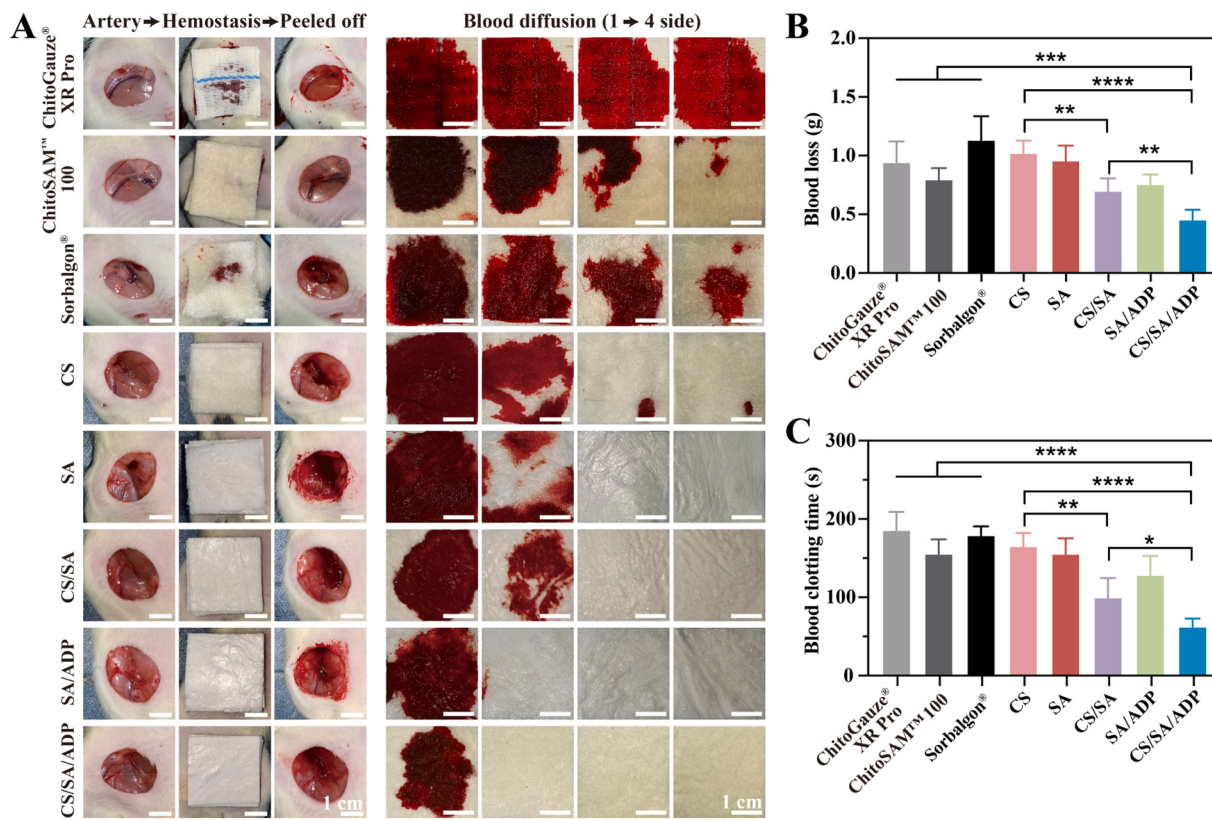


Fig. 6. Hemostatic evaluation of femoral artery injury in rats. (A) Photographs of hemostasis of rat artery with different hemostatic dressings and the diffusion/permeation of blood in the hemostatic dressing, with the first side as the immediate wound and the fourth side as the outermost layer. Quantification of (B) blood loss and (C) hemostasis time in the rat artery hemorrhage model.

in the CS/SA/ADP group compared to the CS/SA group. The formation of platelet pseudopods may be attributed to ADP binding with platelet surface receptors, which stimulates signaling pathways leading to morphological changes (Fig. 4B) [52,53]. Additionally, quantitative analysis revealed that fewer erythrocytes adhered to CS while CS/SA/ADP exhibited the highest number of erythrocytes adhesion (Fig. 4C and D). This result can be attributed to CS having a relatively smooth surface with maximum porosity and poor interaction with erythrocytes. By contrast, CS/SA/ADP possesses a rough fiber-like structure along with sponge-like characteristics enabling tight attachment of numerous erythrocytes.

Intrinsic and extrinsic coagulation pathways play crucial roles in secondary hemostasis [54]. Thus, the APTT and PT were measured to assess the activation of the coagulation pathway by the CS/SA/ADP hemostatic bandage. As shown in Fig. 4E, the APTT values of CS/SA/ADP were significantly lower compared to those of CS/SA and CS. Similarly, the PT values of CS/SA/ADP were comparable to SA, CS/SA, and SA/ADP but significantly lower than those of CS (Fig. 4F). Moreover, both APTT and PT values in the control group were significantly higher than those in the CS/SA/ADP group. Hence, it can be inferred that the reduction in APTT and PT values observed with CS/SA/ADP may be attributed to synergistic hemostatic effects resulting from the presence of ADP, Ca^{2+} , and alginate, which activate both internal and external coagulation pathways [55–57].

3.4. Evaluation of the peeling force and in vivo hemostatic properties of hemostatic bandages

The challenge faced by current hemostatic materials is the potential tearing of wounds and subsequent pain and secondary bleeding upon material removal after achieving hemostasis [58]. A back skin bleeding model was fabricated on the back of rats to assess the easy of peeling for

the prepared hemostatic bandages (Fig. S4). The prepared hemostatic bandages (CS/SA/ADP) had relatively low peel forces without causing any wound tearing during removal (Figs. 5A, B and S5). The peel force was approximately 5.1, 2.5, and 2.6 times lower than that of ChitoGauze® XR Pro, ChitoSAM™ 100, and CS group, respectively. By contrast, Sorbalgon® had a lower peel force but left more residue in the wound necessitating debridement (Fig. S6). These findings indicated that the prepared hemostatic bandage possesses low adhesion strength and easy peeling properties, which mitigate pain and secondary bleeding associated with material removal post-wound treatment [59].

The hemostatic performance of hemostatic bandages in noncompressible wounds was evaluated by using a rat liver laceration hemorrhage model [60,61]. As shown in Fig. 5C, blood spread rapidly into the ChitoGauze® XR Pro and completely saturated all four sides with a blood loss of 0.83 ± 0.17 g (Fig. 5D). ChitoSAM™ 100 and CS are made of chitosan nonwoven fabric, exhibiting similar blood permeability to Sorbalgon®, as all three penetrated three layers of bandages. However, the rate of blood diffusion and extent of wetting were comparatively smaller for these three groups compared to ChitoGauze® XR Pro. This result may be due to the fact that chitosan fiber fabrics can control bleeding better than chitosan gauze for primary hemostasis. Upon application at the bleeding site, CS/SA prevented blood penetration into other layers; only a small area on one side became soaked, indicating its superior hemostatic effect relative to the CS group. Notably, CS/SA exhibited lower blood loss (0.57 ± 0.15 g) than the CS group (0.74 ± 0.04 g). Furthermore, The CS/SA/ADP significantly enhanced hemostasis by confining blood solely within the first layer of the bandage and limited to a small area, resulting in an approximate blood loss of only 0.32 ± 0.15 g.

As shown in Fig. 5E, the hemostasis time of CS/SA/ADP was 31.2 ± 5.49 s, whereas that of ChitoGauze® XR Pro, ChitoSAM™ 100, and Sorbalgon® ranged from 50 to 105 s. Furthermore, the hemostasis time

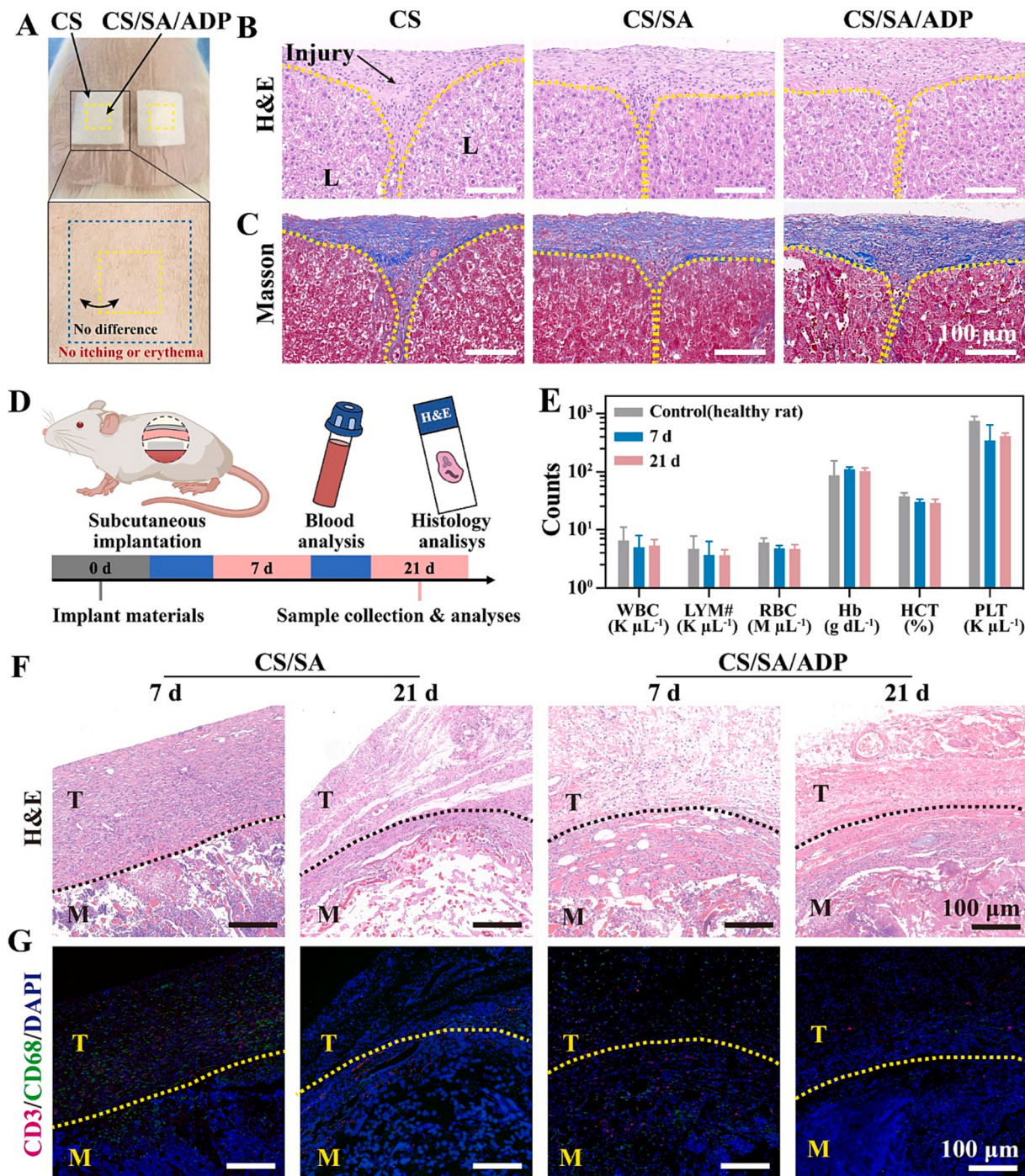


Fig. 7. *In vivo* biocompatibility assessment. (A) Skin compatibility study on rat back. (B) H&E and (C) Masson staining of liver tissue healing at 7 days post-operation. (D) Schematic diagram of hemostatic bandage in a rat subcutaneous model study. (E) Complete blood count of rat blood at 7 and 21 days after implantation of CS/SA/ADP hemostatic bandage. WBC, white blood cells; LYM#, lymphocytes; RBC, red blood cells; Hb, hemoglobin; HCT, hematocrit; PLT, platelets. Representative photographs of (F) H&E and (G) immunofluorescence staining at 7 and 21 days after implantation of hemostatic bandages. T: tissue, M: material, CD3 labeled as lymphocytes, CD68 labeled as macrophages, DAPI labeled as nuclei.

of CS and SA was closer to each other, which was 73.0 ± 12.47 s and 69.2 ± 18.35 s, respectively. The results suggested that the inclusion of sodium alginate, Ca^{2+} , and ADP in hemostatic bandages may enhance procoagulant activity and expedite hemostasis time through synergistic effects [30,62]. It is worth mentioning that the hemostatic time of this hemostatic bandage was improved compared to previously reported ADP or Ca^{2+} doped hemostatic dressings [31,63].

A rat femoral artery injury model was used to assess the hemostatic effect of the hemostatic bandage on a compressible wound. As shown in

Fig. 6A, blood rapidly diffused to all four sides of the ChitoGauze® XR Pro, and there was blood seepage from the seams of the rat's leg (Fig. S7). When employing ChitoSAM® 100 and CS, two layers of the dressing were saturated with blood penetration and diffusion, while only small amounts of blood remained in layers 3 and 4 (Fig. 6B). In contrast, Sorbalgon® exhibited high absorbency during hemostasis, moistening all four layers of the dressing and resulting in a higher blood loss of approximately 1.13 ± 0.20 g. Compared to CS, a minimal amount of blood was observed on the second side of the CS/SA, and blood loss

was reduced to 0.70 ± 0.11 g. In CS/SA/ADP, the blood loss decreased further to 0.45 ± 0.08 g, with only the first layer of the bandage being infiltrated by blood while keeping the other layers dry. Additionally, the shortest hemostasis time was observed in CS/SA/ADP, indicating the strong hemostatic ability (Fig. 6C). Therefore, these findings demonstrated that the CS/SA/ADP hemostatic bandage possesses equivalent efficacy in severe bleeding models involving liver laceration and femoral artery injury.

3.5. In vivo biocompatibility evaluation

In vivo biocompatibility was assessed by adhering a hemostatic bandage to the back skin of rats with a clinically approved medical sterile dressing [64]. As shown in Fig. 7A, no significant irritation, such as erythema itching or cracking (no scratches on the back), was observed in the skin covered with the hemostatic bandage after 24 h of adhesion. H&E staining was employed to assess the impact of residue from the hemostatic bandage on liver wound healing *in vivo*. As shown in Fig. 7B, no discernible pathological alterations were found at the wound site. Notably, the Masson staining results showed that the hemostatic bandage containing ADP promoted wound healing compared with CS nonwoven fabric (Fig. 7C).

In evaluating the biological safety of the materials, the prepared hemostatic bandage was subcutaneously implanted onto the back of rats, and blood samples were regularly collected for hematological analysis and histological examination (Fig. 7D). Blood tests were conducted to evaluate whether degradation of the hemostatic bandage posed any potential systemic toxicity [65]. As shown in Fig. 7E, the degradation products of the hemostatic bandages showed no evident signs of systemic toxicity, and the blood was similar to that of healthy animals. Histological changes in subcutaneous tissues treated with CS/SA and CS/SA/ADP were examined using H&E staining (Fig. 7F). In CS/SA-treated tissues, neutrophil aggregation around the tissue was observed on day 7 post-implantation, indicating a mild local host inflammatory response. Hemostatic bandages containing ADP exhibited reduced recruitment of inflammatory cells. At day 21 after implantation, a small number of inflammatory cells persisted in CS/SA-treated tissues; however, no inflammation was evident in CS/SA/ADP-treated tissues.

The immune response of the hemostatic bandage to subcutaneous implantation was further characterized by immunofluorescence staining for lymphocytes (CD3) and macrophages (CD68). At the junction of CS/SA and subcutaneous tissues, a high amount of CD3 and CD68 infiltration was observed at 7 days, whereas CS/SA/ADP had less inflammatory cell infiltration (Fig. 7G). At 21 days, some inflammatory cells were still present in CS/SA, whereas almost no cells were observed in CS/SA/ADP. These results suggested that the *in vivo* implantation of hemostatic bandages effectively fills both cells and the extracellular matrix within the material interstices, leading to the generation of nascent interconnected tissues rather than a mere formation of a capsule layer. Furthermore, the presence of ADP promotes inflammation resolution and reduces host's inflammatory response. Collectively, these results demonstrated high biocompatibility of the prepared hemostatic bandages.

4. Conclusion

A hemostatic bandage with synergistic advantages was developed for the treatment of acute bleeding wounds. The results showed that the hemostatic bandage not only retained the advantages of sponge in providing a moist environment and absorptivity, but also inherited the breathability and mechanical characteristics of chitosan nonwoven fabric. *In vitro* cellular experiments showed that the hemostatic bandage had high cell compatibility. Moreover, under the synergistic effect of plasma absorption, large aggregation of red blood cells/platelets, and activation of internal/external coagulation cascades, hemostatic bandages can achieve faster hemostasis. The hemostatic bandage

demonstrated significantly superior hemostatic efficacy compared to commercial products such as ChitoGauze® XR Pro, ChitoSAM™ 100, and Sorbalgon® in a severe bleeding model of liver laceration and femoral artery injury in rats. Moreover, the lower peeling force of the hemostatic bandage was effective in preventing adhesion to granulation tissue after hemostasis in a rat dorsal hemorrhage model. Additionally, subcutaneous implantation and blood routine analysis confirmed good biocompatibility of the prepared hemostatic bandage. These results indicate that the prepared hemostatic bandage exhibits a straightforward synthesis process, easy peeling without residue, and good hemostatic properties suitable for emergency applications.

CRediT authorship contribution statement

Jianmin Yang: Conceptualization, Methodology, Formal analysis, Supervision, Funding acquisition, Project administration, Writing – review & editing. **Fengying Cai:** Conceptualization, Investigation, Methodology, Formal analysis, Writing – original draft. **Yicheng Lv:** Conceptualization, Investigation, Formal analysis. **Ting Jiang:** Investigation, Formal analysis. **Xingkai Zhao:** Investigation. **Xueli Hu:** Investigation. **Yunquan Zheng:** Methodology, Resources, Formal analysis. **Xianai Shi:** Conceptualization, Methodology, Supervision, Resources, Project administration.

Declaration of competing interest

The authors declare that they have no known competing financial interests or personal relationships that could have appeared to influence the work reported in this paper.

Data availability

Data will be made available on request.

Acknowledgments

This work was supported by the Nature Sciences Funding of Fujian Province (2022J01095) and Special Fund for Marine Development of Fujian Province (FJHJF-L-2022-4).

Appendix A. Supplementary data

Supplementary data to this article can be found online at <https://doi.org/10.1016/j.ijbiomac.2023.128561>.

References

- [1] P.C. Spinella, A.P. Cap, Prehospital hemostatic resuscitation to achieve zero preventable deaths after traumatic injury, *Curr. Opin. Hematol.* 24 (6) (2017) 529–535.
- [2] D.S. Kauvar, R. Lefering, C.E. Wade, Impact of hemorrhage on trauma outcome: an overview of epidemiology, clinical presentations, and therapeutic considerations, *J. Trauma* 60 (6) (2006) S3–S11.
- [3] K. Brohi, Make the bleeding stop, *Sci. Transl. Med.* 7 (277) (2015), 277fs10.
- [4] B. Guo, R. Dong, Y. Liang, M. Li, Haemostatic materials for wound healing applications, *Nat. Rev. Chem.* 5 (11) (2021) 773–791.
- [5] Q. Zeng, X. Qi, G. Shi, M. Zhang, H. Haick, Wound dressing: from nanomaterials to diagnostic dressings and healing evaluations, *ACS Nano* 16 (2) (2022) 1708–1733.
- [6] C. Hui, L. Ding, T. Sun, Z. Liu, S. Ramakrishna, Y. Long, J. Zhang, Collocaia birds inspired Janus-structured bandage with strong wet tissue adhesion for rapid hemostasis and wound healing, *Chem. Eng. J.* 464 (2023), 142458.
- [7] Y. Wang, D. Xiao, H. Yu, Y. Zhong, L. Zhang, X. Sui, B. Wang, X. Feng, H. Xu, Z. Mao, Composite hydrogel based oxidized sodium carboxymethyl cellulose and gelatin loaded carboxymethylated cotton fabric for hemostasis and infected wound treatment, *Int. J. Biol. Macromol.* 224 (2023) 1382–1394.
- [8] Y. Wang, P. Zhou, D. Xiao, Y. Zhu, Y. Zhong, J. Zhang, X. Sui, X. Feng, H. Xu, Z. Mao, Chitosan-bound carboxymethylated cotton fabric and its application as wound dressing, *Carbohyd. Polym.* 221 (2019) 202–208.
- [9] H. He, W. Zhou, J. Gao, F. Wang, S. Wang, Y. Fang, Y. Gao, W. Chen, W. Zhang, Y. Weng, Z. Wang, H. Liu, Efficient, biosafe and tissue adhesive hemostatic cotton gauze with controlled balance of hydrophilicity and hydrophobicity, *Nat. Commun.* 13 (1) (2022) 552.

- [10] Y. Chen, L. Wu, P. Li, X. Hao, X. Yang, G. Xi, W. Liu, Y. Feng, H. He, C. Shi, Polysaccharide based hemostatic strategy for ultrarapid hemostasis, *Macromol. Biosci.* 20 (4) (2020) 1900370.
- [11] Z. Li, A. Milionis, Y. Zheng, M. Yee, L. Codispoti, F. Tan, D. Poulikakos, C.H. Yap, Superhydrophobic hemostatic nanofiber composites for fast clotting and minimal adhesion, *Nat. Commun.* 10 (1) (2019) 5562.
- [12] Y. Kong, W. Zhang, T. He, X. Yang, W. Bi, J. Li, W. Yang, W. Chen, Asymmetric wettable polycaprolactone-chitosan/chitosan oligosaccharide nanofibrous membrane as antibacterial dressings, *Carbohyd. Polym.* 304 (2023), 120485.
- [13] Z. Li, J. Chen, W. Cao, D. Wei, A. Zheng, Y. Guan, Permanent antimicrobial cotton fabrics obtained by surface treatment with modified guanidine, *Carbohyd. Polym.* 180 (2018) 192–199.
- [14] Q. Xu, E. Hu, H. Qiu, L. Liu, Q. Li, B. Lu, K. Yu, F. Lu, R. Xie, G. Lan, Y. Zhang, Catechol-chitosan/carboxymethylated cotton-based Janus hemostatic patch for rapid hemostasis in coagulopathy, *Carbohyd. Polym.* 315 (2023), 120967.
- [15] C. Guo, J. Zhang, X. Feng, Z. Du, Y. Jiang, Y. Shi, G. Yang, L. Tan, Polyhexamethylene biguanide chemically modified cotton with desirable hemostatic, inflammation-reducing, intrinsic antibacterial property for infected wound healing, *Chinese Chem. Lett.* 33 (6) (2022) 2975–2981.
- [16] X. Yang, N. Shi, J. Liu, Q. Cheng, G. Li, J. Lyu, F. Ma, X. Zhang, 3D printed hybrid aerogel gauzes enable highly efficient hemostasis, *Adv. Healthc. Mater.* 12 (1) (2023), e2201591.
- [17] M.A. Khan, M. Mujahid, A review on recent advances in chitosan based composite for hemostatic dressings, *Int. J. Biol. Macromol.* 124 (2019) 138–147.
- [18] M. Ji, J. Li, Y. Wang, F. Li, J. Man, J. Li, C. Zhang, S. Peng, S. Wang, Advances in chitosan-based wound dressings: modifications, fabrications, applications and prospects, *Carbohyd. Polym.* 297 (2022), 120058.
- [19] H. Hu, F. Luo, Q. Zhang, M. Xu, X. Chen, Z. Liu, H. Xu, L. Wang, F. Ye, K. Zhang, B. Chen, S. Zheng, J. Jin, Berberine coated biocomposite hemostatic film based alginate as absorbable biomaterial for wound healing, *Int. J. Biol. Macromol.* 209 (2022) 1731–1744.
- [20] J. Jin, Z. Ji, M. Xu, C. Liu, X. Ye, W. Zhang, S. Li, D. Wang, W. Zhang, J. Chen, F. Ye, Z. Lv, Microspheres of carboxymethyl chitosan, sodium alginate, and collagen as a hemostatic agent *in vivo*, *ACS Biomater. Sci. Eng.* 4 (7) (2018) 2541–2551.
- [21] M.A. Hassan, T.M. Tamer, K. Valachová, A.M. Omer, M. El-Shafeey, M.S.M. Eldin, L. Soltes, Antioxidant and antibacterial polyelectrolyte wound dressing based on chitosan/hyaluronan/phosphatidylcholine dihydroquercetin, *Int. J. Biol. Macromol.* 166 (2021) 18–31.
- [22] L. Yu, X. Shang, H. Chen, L. Xiao, Y. Zhu, J. Fan, A tightly-bonded and flexible mesoporous zeolite-cotton hybrid hemostat, *Nat. Commun.* 10 (1) (2019) 1932.
- [23] L. Yu, H. Zhang, L. Xiao, J. Fan, T. Li, A bio-inorganic hybrid hemostatic gauze for effective control of fatal emergency hemorrhage in “platinum ten minutes”, *ACS Appl. Mater. Interfaces* 14 (19) (2022) 21814–21821.
- [24] C. Liu, C. Liu, Z. Shi, Z. Li, X. Wang, F. Huang, Trojan-horse mineralization of trigger factor to impregnate non-woven alginate fabrics for enhanced hemostatic efficacy, *Carbohyd. Polym.* 320 (2023), 121213.
- [25] W. Zhang, J. Wu, L. Yu, H. Chen, D. Li, C. Shi, L. Xiao, J. Fan, Paraffin-coated hydrophobic hemostatic zeolite gauze for rapid coagulation with minimal adhesion, *ACS Appl. Mater. Interfaces* 13 (44) (2021) 52174–52180.
- [26] T. Liu, Z. Zhang, J. Liu, P. Dong, F. Tian, F. Li, X. Meng, Electrospun kaolin-loaded chitosan/PEO nanofibers for rapid hemostasis and accelerated wound healing, *Int. J. Biol. Macromol.* 217 (2022) 998–1011.
- [27] X. Li, P. Lu, H. Jia, G. Li, B. Zhu, X. Wang, F. Wu, Emerging materials for hemostasis, *Coordin. Chem. Rev.* 475 (2023), 214823.
- [28] R.N. Puri, R.W. Colman, M.A. Liberman, ADP-Induced platelet activation, *Crit. Rev. Biochem. Mol.* 32 (6) (1997) 437–502.
- [29] Y. Okamura, S. Katsuno, H. Suzuki, H. Maruyama, M. Handa, Y. Ikeda, S. Takeoka, Release abilities of adenosine diphosphate from phospholipid vesicles with different membrane properties and their hemostatic effects as a platelet substitute, *J. Control. Release* 148 (3) (2010) 373–379.
- [30] S.K. Bandyopadhyay, M. Azharuddin, A.K. Dasgupta, B. Ganguli, S. SenRoy, H. K. Patra, S. Deb, Probing ADP induced aggregation kinetics during platelet-nanoparticle interactions: functional dynamics analysis to rationalize safety and benefits, *Front. Bioeng. Biotech.* 7 (2019) 163.
- [31] Y. Liu, H. Niu, C. Wang, X. Yang, W. Li, Y. Zhang, X. Ma, Y. Xu, P. Zheng, J. Wang, K. Dai, Bio-inspired, bio-degradable adenosine 5'-diphosphate-modified hyaluronic acid coordinated hydrophobic undecanal-modified chitosan for hemostasis and wound healing, *Bioact. Mater.* 17 (2022) 162–177.
- [32] J. Zhou, H. Zhang, M.S. Fareed, Y. He, Y. Lu, C. Yang, Z. Wang, J. Su, P. Wang, W. Yan, K. Wang, An injectable peptide hydrogel constructed of natural antimicrobial peptide j-1 and ADP shows anti-infection, hemostasis, and antiadhesion efficacy, *ACS Nano* 16 (5) (2022) 7636–7650.
- [33] A.S. Montaser, M. Rehan, W.M. El-Senousy, S. Zaghloul, Designing strategy for coating cotton gauze fabrics and its application in wound healing, *Carbohyd. Polym.* 244 (2020), 116479.
- [34] J. Zhang, X. Pei, Y. Liu, X. Ke, Y. Peng, Y. Weng, Q. Zhang, J. Chen, Combining chitosan, stearic acid, and (Cu-, Zn-) MOFs to prepare robust superhydrophobic coatings with biomedical multifunctionalities, *Adv. Healthc. Mater.* 12 (30) (2023), e2300746.
- [35] N. Wang, S. Zhao, X. Tian, S. Guang, H. Xu, Fabrication of microspheres containing coagulation factors by reverse microemulsion method for rapid hemostasis and wound healing, *Colloid. Surface. B.* 218 (2022), 112742.
- [36] J. Tang, H. Guan, W. Dong, Y. Liu, J. Dong, L. Huang, J. Zhou, S. Lu, Application of compound polymyxin b ointment in the treatment of chronic refractory wounds, *Int. J. Low. Extr. Wound.* 21 (3) (2022) 320–324.
- [37] C. Lin, W. Shaoyan, Z. Cangming, W. Qi, Comparative study on bulk and composite fibrous samples photophysical feature: synthesis and characterization of a fluorine-containing re(I) complex and its electrospinning fibers, *Spectrochim. Acta A* 142 (2015) 43–49.
- [38] E. Pinho, G. Soares, Functionalization of cotton cellulose for improved wound healing, *J. Mater. Chem. B* 6 (13) (2018) 1887–1898.
- [39] Y. Song, S. Li, H. Chen, X. Han, G.J. Duns, W. Dessie, W. Tang, Y. Tan, Z. Qin, X. Luo, Kaolin-loaded carboxymethyl chitosan/sodium alginate composite sponges for rapid hemostasis, *Int. J. Biol. Macromol.* 233 (2023), 123532.
- [40] R. Dong, H. Zhang, B. Guo, Emerging hemostatic materials for non-compressible hemorrhage control, *Natl. Sci. Rev.* 9 (11) (2022), nwac162.
- [41] M. Li, G. Pan, Y. Yang, B. Guo, Smart aligned multi-layered conductive cryogels with hemostasis and breathability for coagulopathy epistaxis, nasal mucosal repair and bleeding monitoring, *Nano Today* 48 (2023), 101720.
- [42] X. Zhang, K. Dai, C. Liu, H. Hu, F. Luo, Q. Qi, L. Wang, F. Ye, J. Jin, J. Tang, F. Yang, Berberine-coated biomimetic composite microspheres for simultaneous hemostatic and antibacterial performance, *Polymers (Basel)* 13 (3) (2021) 360.
- [43] R.R. Ahmad, W.N. Wan, R.R. Nasaruddin, Alginate and alginate composites for biomedical applications, *Asian. J. Pharm. Sci.* 16 (3) (2021) 280–306.
- [44] F. Ahmad, B. Mushtaq, S. Ahmad, A. Rasheed, Y. Nawab, A novel composite of hemp fiber and alginate hydrogel for wound dressings, *J. Polym. Environ.* 31 (6) (2023) 2294–2305.
- [45] J. Yang, Y. Huang, J. Dai, X. Shi, Y. Zheng, A sandwich structure composite wound dressing with firmly anchored silver nanoparticles for severe burn wound healing in a porcine model, *Regen. Biomater.* 8 (4) (2021), rbab037.
- [46] Y. Yang, M. Li, G. Pan, J. Chen, B. Guo, Multiple stimuli-responsive nanozyme-based cryogels with controlled NO release as self-adaptive wound dressing for infected wound healing, *Adv. Funct. Mater.* 33 (31) (2023) 2214089.
- [47] J. Shen, P.E. DiCorleto, ADP stimulates human endothelial cell migration via P2Y1 nucleotide receptor-mediated mitogen-activated protein kinase pathways, *Circ. Res.* 102 (4) (2008) 448–456.
- [48] P.A. Borges, I. Waclawiak, J.L. Georgii, V.D.S. Fraga-Junior, J.F. Barros, F. S. Lemos, T. Russo-Abrahão, E.M. Saraiva, C.M. Takiya, R. Coutinho-Silva, C. Penido, C. Mermelstein, J.R. Meyer-Fernandes, F.B. Canto, J.S. Neves, P.A. Melo, C. Canetti, C.F. Benjamin, Adenosine diphosphate improves wound healing in diabetic mice through P2Y(12) receptor activation, *Front. Immunol.* 12 (2021), 651740.
- [49] Y. Feng, X. Luo, F. Wu, H. Liu, E. Liang, R. He, M. Liu, Systematic studies on blood coagulation mechanisms of halloysite nanotubes-coated PET dressing as superior topical hemostatic agent, *Chem. Eng. J.* 428 (2022), 132049.
- [50] L.W. Chan, C.H. Kim, X. Wang, S.H. Pun, N.J. White, T.H. Kim, PolySTAT-modified chitosan gauzes for improved hemostasis in external hemorrhage, *Acta Biomater.* 31 (2016) 178–185.
- [51] Y. Feng, Y. He, X. Lin, M. Xie, M. Liu, Y. Lvov, Assembly of clay nanotubes on cotton fibers mediated by biopolymer for robust and high-performance hemostatic dressing, *Adv. Healthc. Mater.* 12 (1) (2023), e2202265.
- [52] L. Dong, X. Liu, S. Wu, Y. Mei, M. Liu, Y. Dong, J. Huang, Y. Li, Y. Huang, Y. Wang, S. Liao, Rhizoma bletillae polysaccharide elicits hemostatic effects in platelet-rich plasma by activating adenosine diphosphate receptor signaling pathway, *Biomed. Pharmacother.* 130 (2020), 110537.
- [53] E.M. Golebiewska, A.W. Poole, Platelet secretion: from haemostasis to wound healing and beyond, *Blood Rev.* 29 (3) (2015) 153–162.
- [54] J. Li, X. Sun, K. Zhang, G. Yang, Y. Mu, C. Su, J. Pang, T. Chen, X. Chen, C. Feng, Chitosan/diatom-biosilica aerogel with controlled porous structure for rapid hemostasis, *Adv. Healthc. Mater.* 9 (21) (2020), e2000951.
- [55] X. Lu, Z. Liu, Q. Jia, W. Wang, Q. Zhang, X. Li, J. Yu, B. Ding, Flexible bioactive glass nanofiber-based self-expanding cryogels with superelasticity and bioadhesion enabling hemostasis and wound healing, *ACS Nano* 17 (12) (2023) 11507–11520.
- [56] T. Qin, X. Huang, Q. Zhang, F. Chen, J. Zhu, Y. Ding, Hemostatic effects of Fmoc-ADP hydrogel consisted of Fmoc-phenylalanine and ADP, *Amino Acids* 55 (4) (2023) 499–507.
- [57] M.N. Sundaram, U. Mony, P.K. Varma, J. Rangasamy, Vasoconstrictor and coagulation activator entrapped chitosan based composite hydrogel for rapid bleeding control, *Carbohyd. Polym.* 258 (2021), 117634.
- [58] S. Li, A. Chen, Y. Chen, Y. Yang, Q. Zhang, S. Luo, M. Ye, Y. Zhou, Y. An, W. Huang, T. Xuan, Y. Pan, X. Xuan, H. He, J. Wu, Lotus leaf inspired antiadhesive and antibacterial gauze for enhanced infected dermal wound regeneration, *Chem. Eng. J.* 402 (2020), 126202.
- [59] X. Jia, C. Hua, F. Yang, X. Li, P. Zhao, F. Zhou, Y. Lu, H. Liang, M. Xing, G. Lyu, Hydrophobic aerogel-modified hemostatic gauze with thermal management performance, *Bioact. Mater.* 26 (2023) 142–158.
- [60] Y. Lv, F. Cai, Y. He, L. Li, Y. Huang, J. Yang, Y. Zheng, X. Shi, Multi-crosslinked hydrogels with strong wet adhesion, self-healing, antibacterial property, reactive oxygen species scavenging activity, and on-demand removability for seawater-immersed wound healing, *Acta Biomater.* 159 (2023) 95–110.
- [61] J. Li, X. Sun, J. Dai, J. Yang, L. Li, Z. Zhang, J. Guo, S. Bai, Y. Zheng, X. Shi, Biomimetic multifunctional hybrid sponge via enzymatic cross-linking to accelerate infected burn wound healing, *Int. J. Biol. Macromol.* 225 (2023) 90–102.
- [62] G. Hollopeter, H.M. Jantzen, D. Vincent, G. Li, L. England, V. Ramakrishnan, R. B. Yang, P. Nurden, A. Nurden, D. Julius, P.B. Conley, Identification of the platelet ADP receptor targeted by antithrombotic drugs, *Nature* 409 (6817) (2001) 202–207.

- [63] Y. Wang, P. Zhou, D. Xiao, Y. Liu, Y. Zhong, B. Wang, L. Zhang, Z. Chen, X. Sui, X. Feng, Calcium functioned carboxymethylated cotton fabric for hemostatic wound dressing, *Cellulose* 27 (2020) 10139–10149.
- [64] A. Momeni, M.J. Filaggi, Degradation and hemostatic properties of polyphosphate coacervates, *Acta Biomater.* 41 (2016) 328–341.
- [65] J. Wu, H. Yuk, T.L. Sarrafian, C. Guo, L.G. Griffiths, C. Nabzdyk, X. Zhao, An off-the-shelf bioadhesive patch for sutureless repair of gastrointestinal defects, *Sci. Transl. Med.* 14 (630) (2022), eabh2857.

Update

International Journal of Biological Macromolecules

Volume 297, Issue , March 2025, Page

DOI: <https://doi.org/10.1016/j.ijbiomac.2025.139804>



Corrigendum

Corrigendum to “Chitosan nonwoven fabric composited calcium alginate and adenosine diphosphate as a hemostatic bandage for acute bleeding wounds” [Int. J. Biol. Macromol. 257 (2024) 128561]



Jianmin Yang ^{a,b,*}, Fengying Cai ^a, Yicheng Lv ^a, Ting Jiang ^a, Xingkai Zhao ^a, Xueli Hu ^a, Yunquan Zheng ^b, Xianai Shi ^{a,b,*}

^a College of Biological Science and Engineering, Fuzhou University, No. 2 Xueyuan Road, Fuzhou 350108, China

^b Fujian Key Laboratory of Medical Instrument and Pharmaceutical Technology, Fuzhou University, No. 2 Xueyuan Road, Fuzhou 350108, China

The authors regret the inclusion of incorrect images for a subpart of Fig. 2. Some cell live/dead staining and migration images were mistakenly submitted due to an error during figure compilation. This was an unintentional oversight and a result of human error. The

corrected Fig. 2 is provided in this corrigendum. The authors confirm that this correction does not alter the results or conclusions of this article.

The authors would like to apologise for any inconvenience caused.

DOI of original article: <https://doi.org/10.1016/j.ijbiomac.2023.128561>.

* Corresponding authors at: College of Biological Science and Engineering, Fuzhou University, No. 2 Xueyuan Road, Fuzhou 350108, China.

E-mail addresses: jmyang@fzu.edu.cn (J. Yang), shixa@fzu.edu.cn (X. Shi).

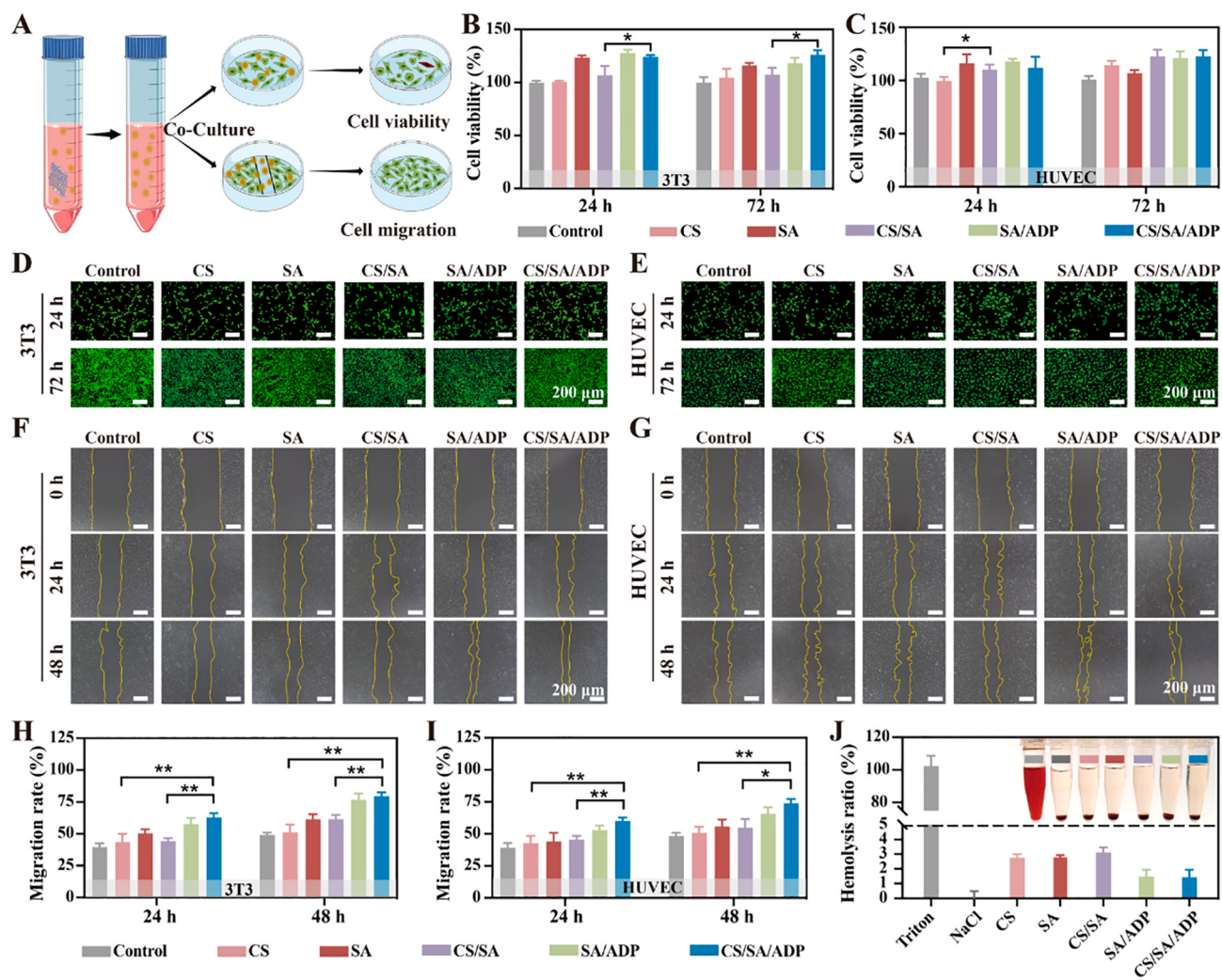


Fig. 2. Cytocompatibility and hemolytic assays of hemostatic bandages. (A) Schematic diagram of the co-culture of material extract and cells. The cell survival rate of (B) 3T3 and (C) HUVEC cells. Live/dead staining analysis of (D) 3T3 and (E) HUVEC cells. (F & G) Migration images and (H & I) migration rates of 3T3 and HUVEC cells. (J) Hemolysis rate of different hemostatic bandages.